Palaeontology
The Palaeontological Association
www.palass.org
[Palaeontology, 2024, e12690]

Forged soft tissues revealed in the oldest fossil reptile from the early Permian of the Alps

by VALENTINA ROSSI[1,2]*, MASSIMO BERNARDI[3], MARIAGABRIELLA FORNASIERO[4], FABRIZIO NESTOLA[5], RICHARD UNITT[2], STEFANO CASTELLI[5] *and* EVELYN KUSTATSCHER[1]

[1]Museum of Nature South Tyrol, Bolzano, Italy; evelyn.kustatscher@naturmuseum.it
[2]School of Biology, Earth and Environmental Sciences, University College Cork, Cork, Ireland; valentina.rossi@ucc.ie, r.unitt@ucc.ie
[3]MUSE – Museo delle Scienze di Trento, Trento, Italy; massimo.bernardi@muse.it
[4]Sezione di Geologia e Paleontologia del Museo della Natura e dell'Uomo, Università degli Studi di Padova, Padua, Italy; mariagabriella.fornasiero@unipd.it
[5]Dipartimento di Geoscienze, Università degli Studi di Padova, Padua, Italy; fabrizio.nestola@unipd.it, stefano.castelli@unipd.it
*Corresponding author

Typescript received 26 September 2023; accepted in revised form 15 December 2023

Abstract: *Tridentinosaurus antiquus* represents one of the oldest fossil reptiles and one of the very few skeletal specimens with evidence of soft tissue preservation from the Cisuralian (Early Permian) of the Italian Alps. The preservation and appearance of the fossil have puzzled palaeontologists for decades and its taphonomy and phylogenetic position have remained unresolved. We reanalysed *T. antiquus* using ultraviolet light (UV), 3D surface modelling, scanning electron microscopy coupled with energy dispersive spectroscopy (SEM-EDS), micro x-ray diffraction (μ-XRD), Raman and attenuated total reflectance Fourier transformed infrared (ATR-FTIR) spectroscopy to determine the origin of the body outline and test whether this represents the remains of organically preserved soft tissues which in turn could reveal important anatomical details about this enigmatic protorosaur. The results reveal, however, that the material forming the body outline is not fossilized soft tissues but a manufactured pigment indicating that the body outline is a forgery. Our discovery poses new questions about the validity of this enigmatic taxon.

Key words: taphonomy, soft tissue preservation, forgery, fossil, Permian, spectroscopy.

THE study of the evolution of reptiles is a prominent research field in palaeontology, but the diversity of early reptile-like animals is still poorly understood. The onset of reptiles occurred at the transition from the Carboniferous to the Permian with fossil localities occurring all around the world. In the Alps, Permian fossiliferous sites yield mostly trackways (Leonardi *et al.* 1974; Conti *et al.* 1975, 1977; Ceoloni *et al.* 1988; Bernardi *et al.* 2017a, 2017b) (e.g. in Italian literature Val Gardena Sandstone, in German literature Gröden Formation) and very rare body fossils (i.e. skeletons). A small lizard-like reptile with a slender body, relatively long neck and pentadactyl limbs, however, was found in Trentino-Alto Adige in 1931 in a fine-grained layer of tuffaceous sandstone (estimated age Cisuralian; 298–273 Ma) and was given the name *Tridentinosaurus antiquus* (Leonardi 1959). *Tridentinosaurus antiquus* (Fig. 1A) was officially described by Leonardi (1959) as an exceptionally preserved fossil showing a dark-coloured body outline associated with an articulated skeleton contrasting with the surrounding pale-pink coloured tuffaceous sandstone. The body outline was interpreted as the remains of soft tissues preserved via 'carbonization' (i.e. organic preservation of soft tissues). Although the overall shape of the fossil is clearly visible, the skeletal elements are not. The long bones of the hindlimbs (i.e. femurs, tibiae and fibulae) are poorly preserved, barely visible on the surface of the rock and no other skeletal elements are recognizable (notably, the skull bones are missing). The description of the taxon and its assignation first to the Araeoscelidae (Leonardi 1959) and then to the polyphyletic group Protorosauria (Dalla Vecchia 1997) were based exclusively on the gross morphology of the body given by the visible dark-coloured body outline. Despite this, the taxon has been reported in other studies (Ronchi *et al.* 2011; Spindler *et al.* 2018, 2019) as an exceptionally preserved key specimen for understanding the diversity of early Permian fauna. However, *T. antiquus* has never been analysed in detail using modern analytical techniques, and its taphonomy and phylogenetic position are unknown. Organically preserved soft tissues can reveal biological information about ancient animals (Vinther 2015; Gabbott *et al.* 2016; McNamara

doi: 10.1111/pala.12690

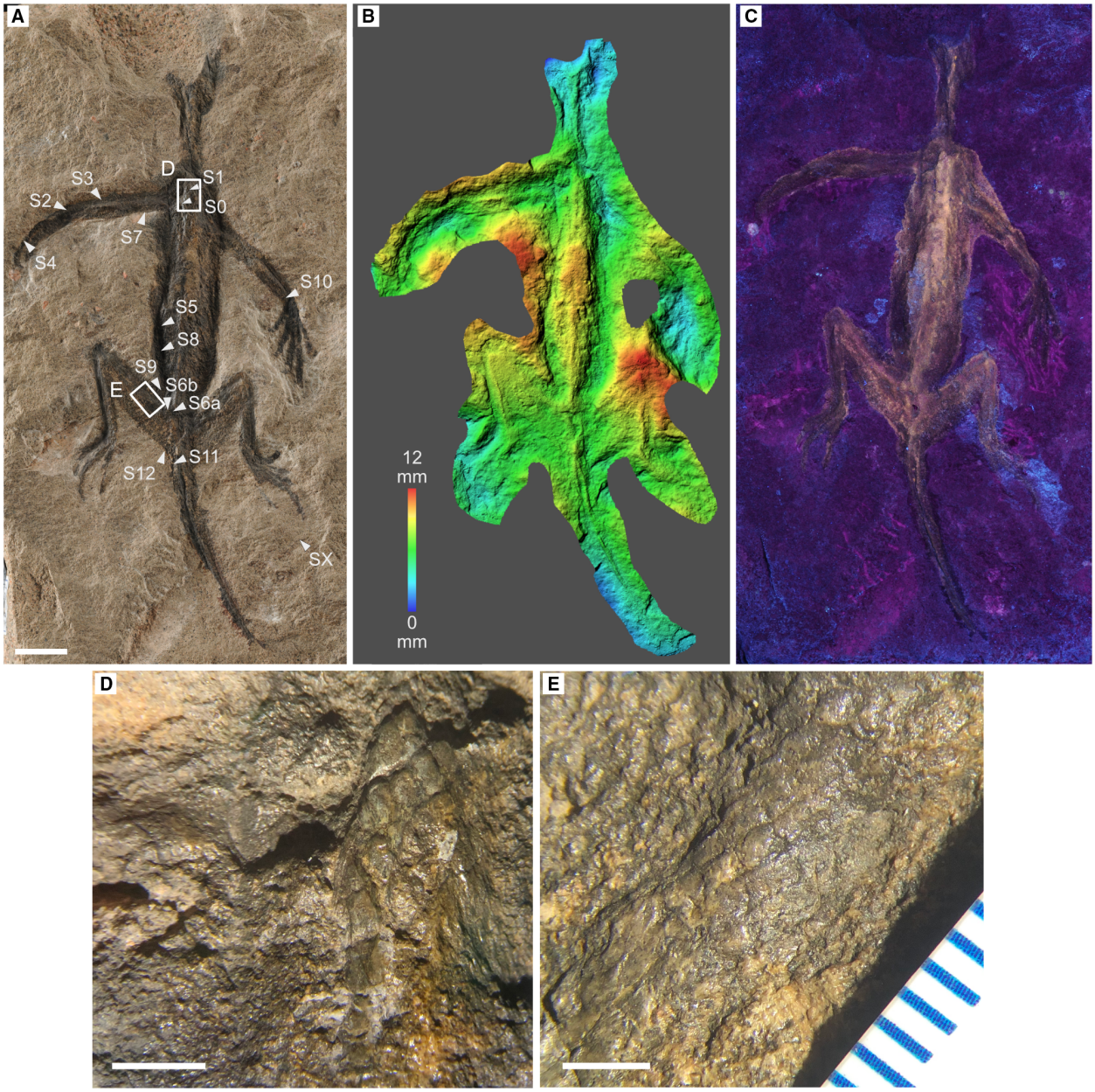

FIG. 1. *Tridentinosaurus antiquus*. A, photograph of the specimen, including sampling locations S0–S12 and SX (matrix). B, map of the topography of the surface of the specimen, highlighting the superficial topography. C, UV photograph showing that the fluorescence of the whole specimen. D, enlargement of the shoulder region, outlined on A. E, enlargement of the pelvic girdle region, outlined on A. Scale bars represent: 20 mm (A); 5 mm (D); 3 mm (E).

et al. 2016a; Spindler *et al.* 2018; Manning *et al.* 2019; Rossi *et al.* 2022; Slater *et al.* 2023), including phylogenetic affinities (Clements *et al.* 2016; Miyashita *et al.* 2019; Rogers *et al.* 2019), and provide important insights into the taphonomic processes that occurred during fossilization. They are thus important to better constrain the diagenetic history of a fossil (Ma *et al.* 2015; McNamara *et al.* 2016b; Rossi *et al.* 2020; Rogers *et al.* 2021).

Here, we focus on characterizing the soft tissues via a multi-technique approach using ultraviolet light (UV), 3D surface modelling, scanning electron microscopy coupled with energy dispersive spectroscopy (SEM-EDS), micro x-ray diffraction (μ-XRD), micro-Raman and attenuated total reflectance Fourier transformed infrared (ATR-FTIR) spectroscopy to study the preservation of the body outline at the physical and chemical level. We tested

the initial hypothesis (Leonardi 1959) that the body outline represents the remains of organically preserved integument and potentially other soft tissues.

GEOLOGICAL SETTING

The fossil was collected from near the 'Stramaiolo' (Redebus) locality in the Pinè Valley. Here, a several-metre-thick fine-grained pyroclastic succession, part of the Regnana Formation, lies stratigraphically below the Ora Formation (Marocchi *et al.* 2008; Morelli *et al.* 2012). The Regnana Formation is generally characterized by a dome of andesitic lava flows (Abbà *et al.* 2018) but locally, distally deposited pyroclastic intercalations are present. The entire succession is part of the southern margin of the Athesian Volcanic Complex (Morelli *et al.* 2012). From the same geographical area where the *T. antiquus* was recovered, fossil plant material comprising large shoot and leaf fragments possibly preserved coalified were also reported (Leonardi 1959). The fossil is hypothesized to be late Kungurian in age, since the overlaying Ora Formation has been dated to 274.1 ± 1.6 Ma (Marocchi *et al.* 2008; Morelli *et al.* 2012).

MATERIAL AND METHOD

Fossil specimen. The hand specimen is housed in the collections of the Museo della Natura e dell'Uomo (MGP-PD 26567; inventory number 5597). The specimen (280 × 220 × 100 mm, 9 kg) was photographed and the body outline was assessed using a Leica 165 C stereo microscope. Regions of interests (n = 13) were identified before sampling (Fig. 1; Table S1). Small samples (1–2 mm^2; n = 18) were dissected from the body outline using sterile tools. Not all samples could be used for all methods due to different preparation requirements. Most samples (n = 13) were placed on carbon tape, coated with Au/Pd and screened using the SEM. A subset of these samples (n = 5) was then prepared for thin sections. Three samples, including the sediment were placed in small plastic capsules for XRD analysis. One sample from the body outline (region S8, 'abdomen') and one sample from the rock were placed in sterile glass vials for ATR-FTIR analysis. We compared the FTIR results of the fossil material with modern melanosomes extracted from the skin of an extant reptile (*Basiliscus basiliscus*; melanosome morphology and chemistry are published in Rossi *et al.* 2019) and a carbon-based manufactured pigment (Bone Black PBk9, Daler Rowney) purchased in a local shop.

Photography and 3D modelling. The specimen was first photographed under white light using a Nikon D300, objective Micro nikkor 60 mm F/2.8 and then photographed under UV light (Way Too Cool, LLC, 95 W, https://www.fluorescents.com); no yellow filter was applied during UV photography. Photographs were then processed in Adobe Photoshop (release 24.05.0). A photogrammetric map and 3D model were built using two dataset of photographs: (1) for the photogrammetric mapping, 90 photographs were taken and the image was produced using Agisoft Metashape Professional (v2.0.1 build 16069); (2) additional photographs, for a total of 110 photographs were used to built the 3D model in Agisoft Metashape Professional (v2.0.1 build 16069). The raw datasets are available in MorphoSource (Rossi & Castelli 2023).

Scanning electron microscopy. Samples were coated in Au/Pb and analysed with a JEOL JSM-6490, in high vacuum at an accelerating voltage of 15 kV, 10 mm working distance. Thin sections were analysed uncoated with a JEOL JSM-IT100, in low vacuum at an accelerating voltage of 10 kV, 10–9 mm working distance.

Thin sections. Samples were embedded in epoxy resin (Araldite 2020, Huntsman), cut and polished until a thickness of 30 µm was reached. Thin sections were photographed using a Nikon Eclipse ME600 optical microscope.

Micro x-ray diffraction. Whole samples were measured using micro x-ray diffraction with a Rigaku Oxford Diffraction SuperNova single-crystal diffractometer working in micro powder diffraction mode, equipped with a Dectris Pilatus 200K area detector and with a MoKα x-ray microsource (working conditions: 50 kV and 0.12 mA). The sample-to-detector distance was 68 mm and x-ray diffraction data were collected for each sample using a 0–360° phi-scan mode with (1 scan per degree) using an exposure time of 40 s per frame.

Micro Raman spectroscopy. Raman spectra were recorded with a Renishaw inVia Qontor Raman Spectrometer System using a 532 nm 50 mW laser. The collected polychromatic light is diffracted by 1800 lines/mm grating, into its constituent wavelengths and captured on a Peltier cooled (−70°C) near infrared enhanced, deep depletion CCD (1024 × 256 pixels). The instrument was calibrated to the 520.5 cm^{-1} line using an integrated silicon standard. Individual spectra were obtained using ×100 objective (0.6 µm spot size); 300 accumulations of 1 s at 5% power. This configuration was chosen to obtain maximum signal to noise ratio whilst avoiding laser induced damage of the material. Spectra were processed in WiRE v5.5 (https://www.renishaw.com) using minimal smoothing, cosmic ray removal and baseline subtraction. The Raman map was obtained using ×50 LWD (long working distance) objective at 10% laser power recording 378 573 spectra at

a spacing of 500 × 500 nm. The map used the Renishaw LiveTrack function of the spectrometer to ensure constant laser focus during data accumulation. The map data were processed in WiRE v5.5, including baseline subtraction, cosmic ray removal and Renishaw's Empty Modelling function to identify and correlate similar spectra.

ATR-FTIR spectroscopy. ATR-FTIR spectroscopy was performed using a Perkir-Elmer Frontier FT-IR/NIR spectrometer equipped with a universal germanium (Ge) diamond-coated crystal. The infrared spectra were collected in the mid-IR range from 4000 to 600 cm^{-1} and 10 accumulations were acquired in attenuated total reflectance with a resolution of 4 cm^{-1}. Spectra were baseline corrected and normalized in SpectrumIR and peak analysis was performed in OriginPro (https://www.originlab.com).

RESULTS

Overall, the specimen presents a great degree of topography (Figs 1A–B, S1; Movie S1). The hindlimbs and tail are topographically higher than the abdomen and forelimbs; the edges of the abdomen are topographically lower than the centre, which in turn is characterized by a ridge. The body outline appears as a dark brown thin film with a slightly glossy appearance; this film is strongly adherent to the rock matrix, which makes the sampling particularly challenging. Discolouration is observed on the upper part of the central ridge and around the hindlimbs. Preparation marks are evident around the forelimbs, especially the right manus and the abdomen. Preliminary investigation using UV photography reveals that the entire specimen, including the bones and body outline (i.e. putative soft tissues), fluoresces as a yellow colour (Fig. 1C). In addition, UV imaging reveals that the perimeter of the body outline is highly irregular (Fig. S2). We tested an organically preserved plant fossil found in the same outcrop where *T. antiquus* was discovered and this specimen did not fluoresce under UV light (Fig. S3).

Microscopic analysis of the specimen reveals novel details about its anatomy. Small rhomboidal scales (max. 2 × 0.9 mm) are found in the region of the shoulder and pelvic girdle (Fig. 1D, E). These show a smooth, partially discoloured surface with a glossy finish. SEM-EDS analysis of small samples from the scales (Fig. S4) shows a thin (*c.* 10 µm) compact C-rich layer on the upper surface; anhedral crystals enriched in Ca and P with no specific microstructure are visible. No other skeletal elements are recognizable on the surface of the rock.

SEM analysis shows that all samples from the body outline comprise angular granules embedded in a microcrystalline matrix associated with other anhedral crystals derived from the matrix (Figs 2, 3, S5). These granules vary in size, measuring from <2 µm up to 20 µm across (Figs 2G–H, 3C–D). Microscopic and SEM analyses of thin sections of selected samples show that these clasts occur within the uneven layer of dark-coloured matter on the surface of the samples (Fig. 3). EDS analysis reveals that these clasts contain exclusively Ca and P, whereas the microcrystalline matrix is associated with Si, O and, to a lesser extent, Al and C (Figs 2I, 3C–D). XRD analysis (Fig. S6) shows the presence of abundant apatite in the samples from the body outline and scales, in addition to quartz, albite, biotite and other phyllosilicates (mainly chlorite). A similar mineralogy is found in the matrix.

Raman mapping (Fig. 4A, B) of one selected thin section confirms the mineralogy of the samples (Fig. S7), but also highlights the presence of an unknown chemical compound associated with the dark-coloured layer. The Raman signature of this compound comprises two broad bands at *c.* 1580 and 1350 cm^{-1} and a peak at *c.* 961 cm^{-1}, although the latter is not always detected (Fig. 4C). The bands are identified as the G (graphite) and D (disorder) bands typical of kerogen, melanin pigments, coal and charcoal, whereas the peak at 961 cm^{-1} is that of apatite. To further investigate this organic signature, ATR-FTIR spectroscopy was used on selected untreated samples from both the matrix and the abdomen (Fig. 4D). The spectrum for the matrix shows major absorption features between 1200 and 400 cm^{-1}. In this range we can assign peaks for the stretching and bending vibrations of the Si–O groups and the Si–O–M group and PO_4^{3-}. These functional groups are typical of quartz, feldspars, phyllosilicates, and apatite (Chukanov & Chervonnyi 2016). A minor spectral feature is the broad band centred at *c.* 3500 cm^{-1} assigned to the stretching and bending vibration of the –OH groups (Chukanov & Chervonnyi 2016). The spectrum from the abdomen shows similar absorption features as the matrix between 1200 and 400 cm^{-1}, but it differs from that for a stronger band for the OH groups, a small shift in the frequency of the sharp peak at *c.* 1090 cm^{-1} and the presence of other peaks in two distinct frequency ranges: (1) between 3000 and 2750 cm^{-1}; and (2) between 1720 and 1420 cm^{-1}. In the first range the peaks at 2930 and 2855 cm^{-1} are assigned to the CH_2 antisymmetric and symmetric stretching vibration, respectively. Several peaks can be assigned in the second frequency range which can be identified as the 'aromatic carbon network' (Van Loon & Boon 2004). This absorption region comprises weak peaks identified using the literature (Daher *et al.* 2011; Daveri *et al.* 2018; Lluveras-Tenorio *et al.* 2019) as follows: the 1713 cm^{-1} peak can be assigned to the stretching mode of C=O bonds; the 1636 cm^{-1} peak can be assigned to the stretching mode of $C=CH_2$; the peak at 1556 cm^{-1} is tentatively assigned to the stretching mode of N–O; the

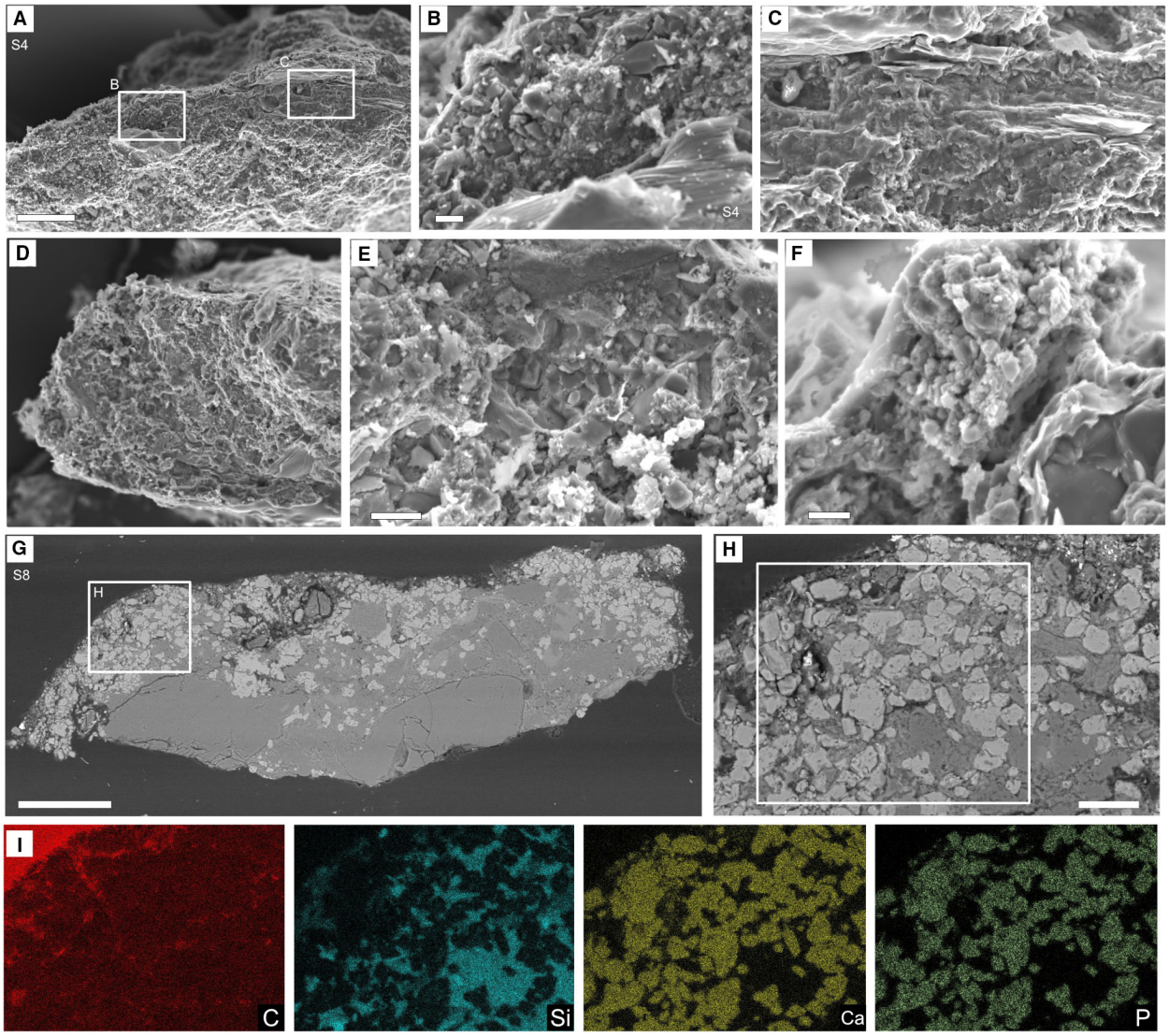

FIG. 2. SEM-EDS analysis of samples from the body outline. A–C, micrographs of sample S4. D–F, micrographs of sample S9. G–H, backscatter image of polished surface of sample S8. I, elemental maps of part of the area shown in H for C, Si, Ca and P. All samples show a microgranular texture and absence of typical soft tissue ultrastructure. Scale bars represent: 50 μm (A, D, E); 20 μm (C, H); 5 μm (B, F); 100 μm (G).

peak at 1457 cm^{-1} is assigned to the bending deformation of CH bonds and finally at 1416 cm^{-1} can be tentatively assigned to the vibration of CH_2 and CH_3 in alkenes. Furthermore, we analysed a sample of melanosomes extracted from the skin of an extant reptile (Rossi *et al.* 2019) and a sample of commercial black paint (Bone Black PBk9, Daler Rowney) for comparison (Fig. S8). The spectrum of melanosomes exhibits the broad peak at *c.* 3300 cm^{-1}, assigned to OH and N–H bonds, and two peaks at 2924 and 2867 cm^{-1} assigned to CH_2 antisymmetric and symmetric stretching vibration, respectively (Glass *et al.* 2012; Cloete *et al.* 2023). Major peaks centred at 1600, 1462, 1353, 1248 and 1047 cm^{-1} can be respectively assigned to amide I (C=O, C–N), bending deformation of CH bonds, in plane bending mode of OH and N-H, N-H twisting modes and O=C–N bending and finally cysteine S–O and S=O bonds (Pralea *et al.* 2019; Cloete *et al.* 2023), in melanin and proteinaceous matter within melanosomes. The spectrum of bone black paint shows major sharp peaks between 1500 and 1400 cm^{-1} and between 1090 and 800 cm^{-1}. The former frequencies are associated with vibrational modes of C–O bonds in calcium carbonates and CH_2 and CH_3 in alkenes, whereas the latter with P–O and Si–O bonds in apatite and silicate impurities (Lluveras-Tenorio *et al.* 2019) minor peaks at 1647 and 1603 cm^{-1} can be tentavely assigned to

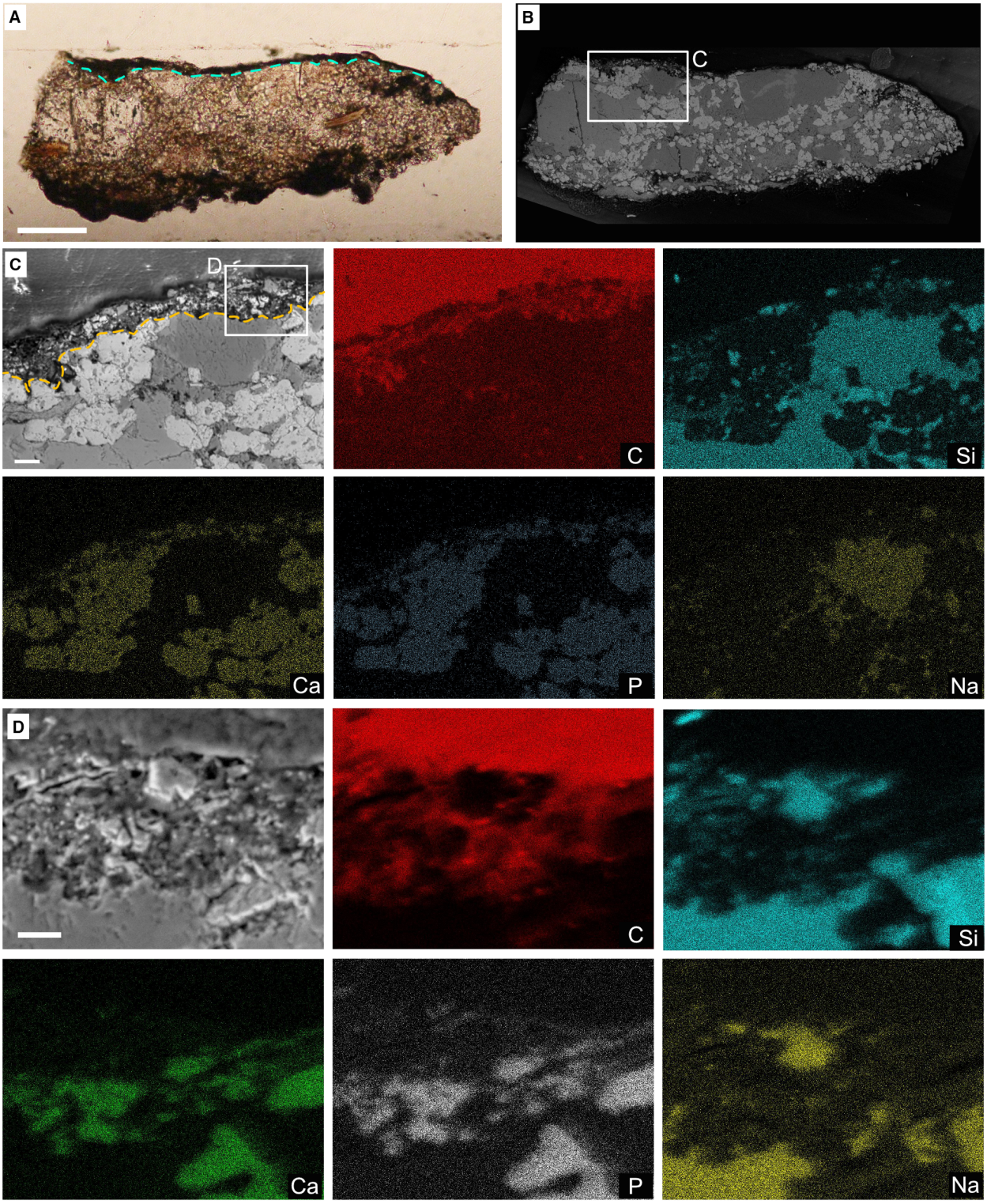

FIG. 3. SEM-EDS analysis of thin section of sample S9. A, photograph of sample S9; dashed line represent layers of dark coloured matter forming the 'body outline'. B, backscattered image of sample S9 showing the irregular thickness and microgranular texture of the 'body outline' layer. C, detailed image of the superficial dark-coloured layer, with associated elemental maps of C, Si, Ca, P and Na. D, close-up of the superficial layer with associated elemental maps of C, Si, Ca, P and Na. Scale bars represent: 100 μm (A); 10 μm (C); 5 μm (D).

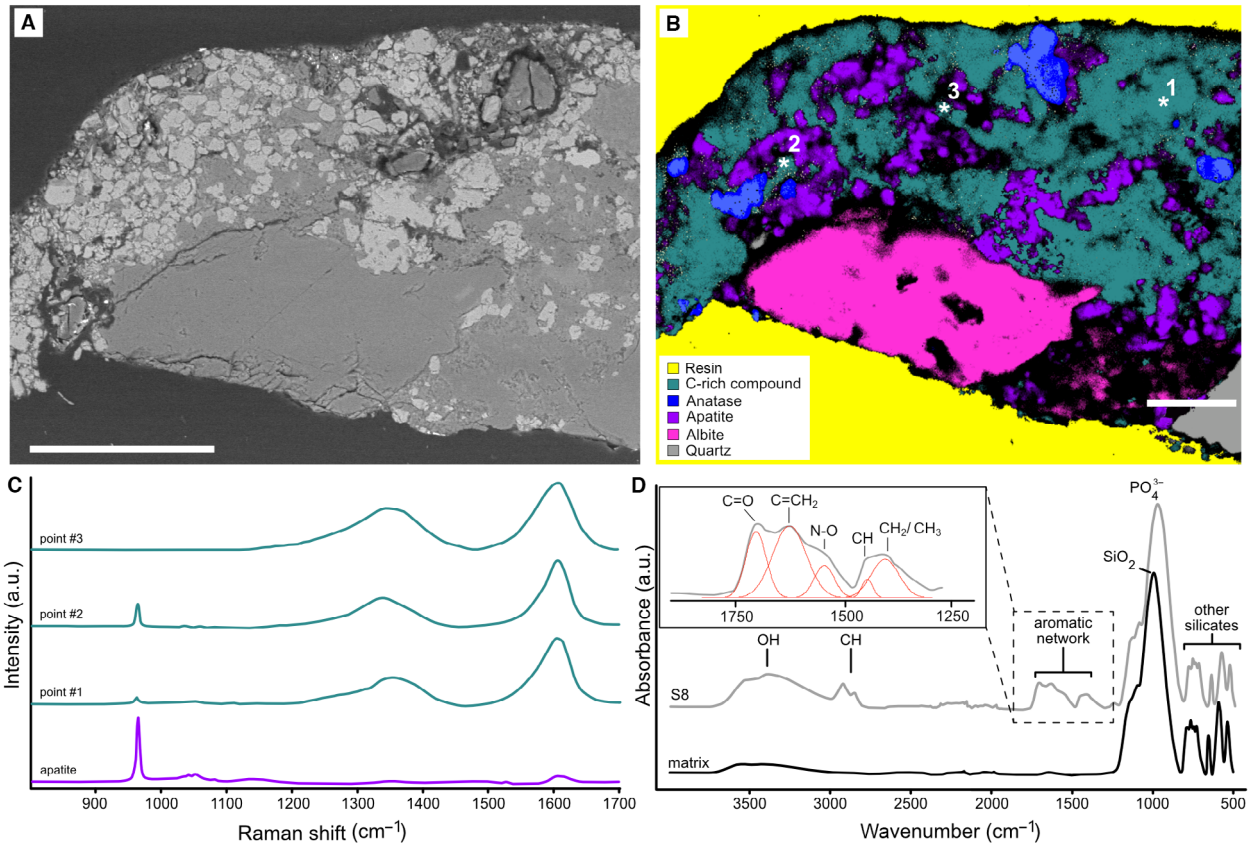

FIG. 4. Micro-Raman and ATR-FTIR spectroscopy of sample from the abdomen. A, SEM backscatter image of a thin section of sample S8. B, Raman map of the same sample in A showing the presence of mineral crystals from the sediment that are covered by a layer comprising a C-rich compound; * denotes points where single spectra where acquired. C, Raman spectra of unknown compound and apatite. D, ATR-FTIR spectra of samples from the abdomen and rock matrix. Scale bars represent: 100 μm (A); 50 μm (B).

proteinaceous residues of the organic binders or the bone fragments (Daveri *et al.* 2018).

Overall, the pattern of peaks in the spectrum of the sample from the abdomen is not comparable with these and with those reported from organically preserved vertebrate soft tissues (i.e. fossilized melanin; Lindgren *et al.* 2012; Barden *et al.* 2015; McNamara *et al.* 2016b; Yang *et al.* 2019; Cincotta *et al.* 2020); instead, our data closely resemble that of the manufactured bone black pigment reported by Van Loon & Boon (2004).

DISCUSSION

Our study sheds light on the origin of the body outline in *T. antiquus*, which was hypothesized to represent organically preserved soft tissues. Small rhomboidal scales described here are interpretated as putative osteoderms that have undergone recrystallization of apatite due to diagenesis, resulting in the loss of the original bone microstructure.

Overall, the specimen lacks the basic characteristics of a fossil vertebrate with organically preserved soft tissues (i.e. compression fossils). Usually, these fossils are flattened and show little topography. Moreover, the organic material associated with soft tissues does not normally fluoresce under UV light. Instead, in *T. antiquus* the area occupied by the purported soft tissues is topographically variable and the dark-coloured material fluoresces under UV light. The variation in topography within the specimen is explained as the result of extensive mechanical preparation, possibly aimed at exposing more of the skeleton, although without much success. Coatings such as lacquers, varnishes, and glues, as well as certain artificial pigments are fluorescent under UV light (Carden 1991; Cosentino 2015). Our results suggest that one or more layers of coating have been applied on the body outline, osteoderms and bones.

Organically preserved soft tissues in fossil vertebrates usually comprise melanosomes (i.e. melanin-containing organelles preserved either three-dimensionally or as external moulds; Vinther *et al.* 2008; Zhang *et al.* 2010;

Lindgren *et al.* 2012; Rossi *et al.* 2019, 2020, 2022; Yang *et al.* 2019; Cincotta *et al.* 2022), but in some rare cases, melanosomes are not physically preserved. In these cases, the C-rich soft tissue remains appear as an amorphous layer, but a melanin chemical signature can still be found (Brown *et al.* 2017; Fabbri *et al.* 2020). In addition, in both cases, C-rich thin films are usually relatively soft and easy to dissect from the surface of the rock (VR pers. obs.). In the present study, the granular aspect of the dark-coloured layer observed in the samples from the body outline is not compatible with textures typical of soft tissue preservation. Instead, the granular texture resembles that of manufactured pigments seen in historical paintings (e.g. Van Loon & Boon 2004). Our combined spectroscopic data failed to provide a chemical signature of fossilized melanin. The Raman spectrum of the sample from the body outline exhibits D and G bands; these bands are characteristic of eumelanin pigments in extant tissues (Capozzi *et al.* 2005; Saha *et al.* 2011), but also of carbon-based manufactured pigment (Tomasini *et al.* 2012) and any disordered carbon solids (e.g. kerogen; Merlen *et al.* 2017; Craddock & Sauerer 2022). In fossilized melanosome-rich tissues, D and G bands have also been reported (Peteya *et al.* 2016; Pinheiro *et al.* 2019; Rossi *et al.* 2022). The presence of weak absorption features in the aromatic region of the FTIR spectrum can indicate the presence of fossilized degradation product of biomolecules (Cincotta *et al.* 2020) but are also typical of organic binders (e.g. linseed oil and animal glues) used to produce the paints (Van Loon & Boon 2004; Vahur *et al.* 2016). The peaks in the aromatic region of the sample from the abdomen, however, are different in shape from those found in the sample of bone black paint analysed here and those reported in the literature (Daveri *et al.* 2018; Lluveras-Tenorio *et al.* 2019) and in online databases (CAMEO https://cameo.mfa.org; Vahur *et al.* 2016); this is likely to be due to differences in binder and pigment purity but could also be the result of the aging of the paint itself (Van Loon & Boon 2004) and/or the use of a second layer of coating (e.g. varnish) on the surface of the rock. These findings, coupled with UV results, the abundance of apatite fragments and the absence of preserved melanosomes and/or a clear C-rich amorphous layer strongly indicate that the material forming the body outline is made of a manufactured carbon-based pigment mixed with an organic binder. Based on our analysis and comparison with the literature (Van Loon & Boon 2004; Tomasini *et al.* 2012; Coccato *et al.* 2015) we identify the body outline as the result of the application of bone black paint on the surface of the rock.

Our results therefore indicate that the purported fossilized soft tissues of *T. antiquus* are not original but are the result of forgery. The paint applied within the prepared area around the poorly preserved bones and osteoderms, produced the shape of a slender lizard-like animal making the specimen look authentic. In addition, since coalified plant material was recovered from similar deposits in the same geographical region, the forged body outline misled previous palaeontologists to interpret this feature as the remains of carbonized soft tissues. The absence of original soft tissue does not allow further clarification about the anatomy, the depositional environment or the diagenetic history of the specimen.

Forgery of fossils is an infamous practice that palaeontologists are facing all around the world (Wang 2013; Pickrell 2014; DeMiguel *et al.* 2021; Romano & Pignatti 2021). Recurrent evidence of forged specimens is found especially in historical collections and often slips undetected by even the most experienced experts. In the field of amber research for instance, specimens are routinely tested using diagnostic methods (i.e. FTIR) to recognize forged specimens before any further analyses of the amber and/or inclusions (Sosiak *et al.* 2023). Skeletons of various fossil animals have been forged using bones from multiple individuals or those of different animals (Rowe *et al.* 2001; Zhou *et al.* 2002; Scheyer *et al.* 2023) but also, bones have been replaced by manufactured ones (e.g. plastic; Stone 2010). Fossils with evidence of soft tissues are also susceptible as soft tissues have been painted over the rock to completely change the aspect of the fossil (Selden *et al.* 2019) or, as in the case of *T. antiquus*, to add on a previously carved body outline.

Forged fossils often lack important information about provenance, stratigraphic position and a record of previous preparation practices performed on the specimen. In the case of *T. antiquus*, the provenance is known (see Geological Setting, above) but there is still some uncertainty as to the precise stratigraphic location of the outcrop; the general age (late Kungurian) is inferred. There are no records about the conservation history and/or previous preparation of the specimen. The putative soft tissues are mentioned in the first official description of the taxon (Leonardi 1959) and thus it is plausible that the forgery took place before that, perhaps executed to embellish the specimen and/or make it more visible on the surface of the rock.

Our findings cast doubt on the validity of the taxon. The establishment of the taxon was based on morphological data derived from the observation of the body proportion and measurements of limbs, neck and abdomen (Leonardi 1959). Poorly preserved bones are visible in the hind limbs, but these lack all diagnostic features (e.g. processes, foramens) that are usually used to classify a taxon. Skeletal elements of the forelimbs and autopodia (i.e. hands and feet) and girdles are not visible and the overall shapes of these are evident due to the black paint and thus cannot be considered as characters. The same is true

for the abdominal region. Vertebrae are not recognizable in the neck and along the tail. Skeletal elements of the skull are absent, and no bone cross-sections are identified along the fracture where the head of the specimen is supposed to be located. These observations question the actual completeness of the skeleton of *T. antiquus*. Based on our results only the proportions of the poorly preserved femurs and tibiae/fibulae can be used in comparative phylogenetic analysis.

CONCLUSION

The application of modern analytical techniques can assist in unmasking and quantifying the extent of forgery, especially in historically collected fossils with a somewhat enigmatic preservation. The putative soft tissues of *T. antiquus*, one of the oldest known reptiles from the Alps, are fake and thus this specimen is not an exceptionally preserved fossil. Despite this, the poorly preserved long bones of the hindlimbs seem to be genuine and resemble the quality of preservation of exposed bones of Late Triassic pterosauromorphs (e.g. *Scleromochlus*; Bennett 2020; Foffa *et al.* 2022). Modern tomographic methods might reveal novel information about the preserved skeleton but, until then, we suggest caution in using *T. antiquus* in phylogenetic studies.

Acknowledgements. We would like to thank the Superintendence of Cultural Heritage of Padova and L. Giusberti for supporting access and sampling of the fossil specimen during Covid restrictions; A. Lorenzetti and S. Kearns for preliminary Raman study and SEM investigation, respectively. D. Hezel for access to the SEM laboratory at the Goethe University (Frankfurt, Germany) during Covid restrictions; L. Tauro for assistance during the preparation of thin sections; B. Paknazar for the video montage; T. Slater for assistance during FTIR analysis. We also thank S. Thomas, P. Gueriau and an anonymous reviewer for their constructive comments and positive feedback. The study of the *Tridentinosaurus antiquus* was funded by the Promotion of Educational Policies, University and Research Department of the Autonomous Province of Bolzano — South Tyrol within the research project 'Living with the supervolcano - How Athesian eruptions destroyed and preserved 15 million years of Permian life' (nr. 11/34; CUP H32F20000010003) awarded to EK. VR is currently supported by an ERC consolidator grant 'Palaeochem': H2020-ERC-COG-101003293 awarded to Prof. M. McNamara (University College Cork). Open access funding provided by IReL.

Author contributions. **Conceptualization** V Rossi (VR), M Bernardi (MB); **Funding acquisition** E Kustatscher (EK); **Methodology** VR (sampling, SEM-EDS, Raman & FTIR spectroscopy, data analysis). S Castelli (SC) (3D modelling & UV), R Unitt (RU) (Raman spectroscopy), F Nestola (FN) (XRD); **Project administration**: EK; **Resources** M Fornasiero (MF); **Writing – Original Draft** VR; **Writing – Review & Editing** VR, MB, MF, FN, RU, SC, EK.

DATA ARCHIVING STATEMENT

Photogrammetry data are available here: https://doi.org/10.17602/M2/M598952

Editor. Kenneth Angielczyk

SUPPORTING INFORMATION

Additional Supporting Information can be found online (https://doi.org/10.1111/pala.12690):

Fig. S1. *T. antiquus* photographed under oblique illumination to highlight the topography of the surface of the specimen.
Fig. S2. Details of the body outline under oblique and UV lights.
Fig. S3. Fossilized plant fragment embedded in a similar rock as that of *T. antiquus* from Pinè Valley.
Fig. S4. SEM analysis of other samples from the osteoderms and body outline.
Fig. S5. SEM analysis of other samples from the body outline.
Fig. S6. Micro x-ray diffractograms collected on samples from the osteoderm, body outline and matrix.
Fig. S7. Raman spectra of resin and minerals present in the sample shown in Figure 4.
Fig. S8. ATR-FTIR spectra of modern melanosome and bone black paint samples.
Table S1. List of samples and analytical techniques.
Movie S1. 3D model of the specimen *T. antiquus*.

REFERENCES

Abbà, T., Breda, A., Massironi, M., Preto, N., Piccin, G., Trentini, T., Bondesan, A., Carton, A., Fontana, A. and Mozzi, P. 2018. Pre-alpine and alpine deformation at San Pellegrino pass (Dolomites, Italy). *Journal of Maps*, **14**, 671–679.

Barden, H. E., Bergmann, U., Edwards, N. P., Egerton, V. M., Manning, P. L., Perry, S., van Veelen, A., Wogelius, R. A. and van Dongen, B. E. 2015. Bacteria or melanosomes? A geochemical analysis of micro-bodies on a tadpole from the Oligocene Enspel Formation of Germany. *Palaeobiodiversity & Palaeoenvironments*, **95**, 33–45.

Bennett, S. C. 2020. Reassessment of the Triassic archosauriform *Scleromochlus taylori*: neither runner nor biped, but hopper. *PeerJ*, **8**, e8418.

Bernardi, M., Petti, F., Citton, P. and Romano, M. 2017a. The tetrapod ichnoassociation of the Bletterbach (Trentino Alto-Adige) and its place among Late Permian terrestrial ecosystems. *GeoAlp*, **14**, 63–83.

Bernardi, M., Petti, F. M., Kustatscher, E., Franz, M., Hartkopf-Fröder, C., Labandeira, C. C., Wappler, T., van Konijnenburg-van Cittert, J. H., Peecook, B. R. and

Angielczyk, K. D. 2017b. Late Permian (Lopingian) terrestrial ecosystems: a global comparison with new data from the low-latitude Bletterbach Biota. *Earth-Science Reviews*, **175**, 18–43.

Brown, C. M., Henderson, D. M., Vinther, J., Fletcher, I., Sistiaga, A., Herrera, J. and Summons, R. E. 2017. An exceptionally preserved three-dimensional armored dinosaur reveals insights into coloration and Cretaceous predator-prey dynamics. *Current Biology*, **27**, 2514–2521.

Capozzi, V., Perna, G., Gallone, A., Biagi, P. F., Carmone, P., Fratello, A., Guida, G., Zanna, P. and Cicero, R. 2005. Raman and optical spectroscopy of eumelanin films. *Journal of Molecular Structure*, **744–747**, 717–721.

Carden, M. L. 1991. Use of ultraviolet light as an aid to pigment identification. *APT Bulletin: The Journal of Preservation Technology*, **23**, 26–37.

Ceoloni, P., Conti, M., Mariotti, N., Mietto, P. and Nicosia, U. 1988. Tetrapod footprint faunas from Southern and Central-Europe. *Zeitschrift für Geologische Wissenschaften*, **16**, 895–906.

Chukanov, N. V. and Chervonnyi, A. D. 2016. *Infrared spectroscopy of minerals and related compounds*. Springer.

Cincotta, A., Nguyen Tu, T. T., Colaux, J. L., Terwagne, G., Derenne, S., Godefroit, P., Carleer, R., Anquetil, C. and Yans, J. 2020. Chemical preservation of tail feathers from *Anchiornis huxleyi*, a theropod dinosaur from the Tiaojishan Formation (Upper Jurassic, China). *Palaeontology*, **63**, 841–863.

Cincotta, A., Nicolaï, M., Campos, H. B. N., McNamara, M., D'Alba, L., Shawkey, M. D., Kischlat, E.-E., Yans, J., Carleer, R. and Escuillié, F. 2022. Pterosaur melanosomes support signalling functions for early feathers. *Nature*, **604**, 684–688.

Clements, T., Dolocan, A., Martin, P., Purnell, M. A., Vinther, J. and Gabbott, S. E. 2016. The eyes of *Tullimonstrum* reveal a vertebrate affinity. *Nature*, **532**, 500–503.

Cloete, K. J., Šmit, Ž. and Gianoncelli, A. 2023. Multidimensional profiling of human body hairs using qualitative and semi-quantitative approaches with SR-Xrf, ATR-Ftir, Dsc, and SEM-EDX. *International Journal of Molecular Sciences*, **24**, 4166.

Coccato, A., Jehlicka, J., Moens, L. and Vandenabeele, P. 2015. Raman spectroscopy for the investigation of carbon-based black pigments. *Journal of Raman Spectroscopy*, **46**, 1003–1015.

Conti, M. A., Leonardi, G., Mariotti, N. and Nicosia, U. 1975. Tetrapod footprints, fishes and molluscs from the middle Permian of the dolomites (N. Italy). *Memorie Geopaleontologiche*, **3**, 139–150.

Conti, M. A., Leonardi, G., Mariotti, N. and Nicosia, U. 1977. Tetrapod footprints of the "Val Gardena Sandstone" (North Italy). Their palaeontological, stratigraphic and palaeoenvironmental meaning. *Palaeontographia Italica*, **70**, 1–91.

Cosentino, A. 2015. Effects of different binders on technical photography and infrared reflectography of 54 historical pigments. *International Journal of Conservation Science*, **6**, 287–298.

Craddock, P. R. and Sauerer, B. 2022. Robust determination of kerogen properties in organic-rich mudrocks via Raman Spectroscopy. *Organic Geochemistry*, **169**, 104381.

Daher, C., Paris, C., Le Hô, A. S., Bellot-Gurlet, L. and Échard, J. P. 2011. A joint use of Raman and infrared spectroscopies for the identification of natural organic media used in ancient varnishes. *Journal of Raman Spectroscopy*, **41**, 1494–1499.

Dalla Vecchia, F. M. 1997. Mesozoic Amphibia and Reptilia stored at the Museum of Paleontology of the University of Padua. *Natura Nascosta*, **15**, 34–43.

Daveri, A., Malagodi, M. and Vagnini, M. 2018. The bone black pigment identification by noninvasive, in situ infrared reflection spectroscopy. *Journal of Analytical Methods in Chemistry*, **2018**, 6595643.

DeMiguel, D., Brilha, J., Alegret, L., Arenillas, I., Arz, J. A., Gilabert, V., Strani, F., Valenciano, A., Villas, E. and Azanza, B. 2021. Linking geological heritage and geoethics with a particular emphasis on palaeontological heritage: the new concept of 'palaeontoethics'. *Geoheritage*, **13**, 1–16.

Fabbri, M., Wiemann, J., Manucci, F. and Briggs, D. E. 2020. Three-dimensional soft tissue preservation revealed in the skin of a non-avian dinosaur. *Palaeontology*, **63**, 185–193.

Foffa, D., Dunne, E. M., Nesbitt, S. J., Butler, R. J., Fraser, N. C., Brusatte, S. L., Farnsworth, A., Lunt, D. J., Valdes, P. J. and Walsh, S. 2022. *Scleromochlus* and the early evolution of Pterosauromorpha. *Nature*, **610**, 313–318.

Gabbott, S. E., Donoghue, P. C., Sansom, R. S., Vinther, J., Dolocan, A. and Purnell, M. A. 2016. Pigmented anatomy in Carboniferous cyclostomes and the evolution of the vertebrate eye. *Proceedings of the Royal Society B*, **283**, 20161151.

Glass, K., Ito, S., Wilby, P. R., Sota, T., Nakamura, A., Bowers, C. R., Vinther, J., Dutta, S., Summons, R. and Briggs, D. E. 2012. Direct chemical evidence for eumelanin pigment from the Jurassic period. *Proceedings of the National Academy of Sciences*, **109**, 10218–10223.

Leonardi, P. 1959. *Tridentinosaurus antiquus* Gb. Dal Piaz rettile protorosauro permiano del trentino orientale. *Memorie degli Istituti di Geologia e Mineralogia degll'Università di Padova*, **21**, 1–17.

Leonardi, P., Conti, M. A., Leonardi, G., Mariotti, N. and Nicosia, U. 1974. *Pachypes dolomiticus* n. gen. n. sp.; Pareiasaur footprint from the "Val Gardena Sandstone" (Middle Permian) in the western Dolomites (N. Italy). *Atti della Accademia Nazionale dei Lincei. Classe di Scienze Fisiche, Matematiche e Naturali. Rendiconti*, **57**, 221–232.

Lindgren, J., Uvdal, P., Sjövall, P., Nilsson, D. E., Engdahl, A., Schultz, B. P. and Thiel, V. 2012. Molecular preservation of the pigment melanin in fossil melanosomes. *Nature Communications*, **3**, 824.

Lluveras-Tenorio, A., Spepi, A., Pieraccioni, M., Legnaioli, S., Lorenzetti, G., Palleschi, V., Vendrell, M., Colombini, M. P., Tinè, M. R. and Duce, C. 2019. A multi-analytical characterization of artists' carbon-based black pigments. *Journal of Thermal Analysis & Calorimetry*, **138**, 3287–3299.

Ma, X., Edgecombe, G. D., Hou, X., Goral, T. and Strausfeld, N. J. 2015. Preservational pathways of corresponding brains of a Cambrian euarthropod. *Current Biology*, **25**, 2969–2975.

Manning, P. L., Edwards, N. P., Bergmann, U., Anné, J., Sellers, W. I., van Veelen, A., Sokaras, D., Egerton, V. M., Alonso-Mori, R. and Ignatyev, K. 2019. Pheomelanin pigment remnants mapped in fossils of an extinct mammal. *Nature Communications*, **10**, 2250.

Marocchi, M., Morelli, C., Mair, V., Klötzli, U. and Bargossi, G. 2008. Evolution of large silicic magma systems: new U-Pb zircon data on the NW Permian Athesian Volcanic Group (Southern Alps, Italy). *The Journal of Geology*, **116**, 480–498.

McNamara, M. E., Orr, P. J., Kearns, S. L., Alcalá, L., Anadón, P. and Peñalver, E. 2016a. Reconstructing carotenoid-based and structural coloration in fossil skin. *Current Biology*, **26**, 1075–1082.

McNamara, M. E., van Dongen, B. E., Lockyer, N. P., Bull, I. D. and Orr, P. J. 2016b. Fossilization of melanosomes via sulfurization. *Palaeontology*, **59**, 337–350.

Merlen, A., Buijnsters, J. G. and Pardanaud, C. 2017. A guide to and review of the use of multiwavelength Raman spectroscopy for characterizing defective aromatic carbon solids: from graphene to amorphous carbons. *Coatings*, **7**, 153.

Miyashita, T., Coates, M. I., Farrar, R., Larson, P., Manning, P. L., Wogelius, R. A., Edwards, N. P., Anné, J., Bergmann, U. and Palmer, A. R. 2019. Hagfish from the Cretaceous Tethys Sea and a reconciliation of the morphological–molecular conflict in early vertebrate phylogeny. *Proceedings of the National Academy of Sciences*, **116**, 2146–2151.

Morelli, C., Marocchi, M., Moretti, A., Bargossi, G. M., Gasparotto, G., Waele, B., Klötzli, U. and Mair, V. 2012. Volcanic stratigraphy and radiometric age constraints at the northern margin of a mega-caldera system: Athesian Volcanic Group (Southern Alps, Italy). *GeoActa*, **11**, 51–67.

Peteya, J. A., Clarke, J. A., Li, Q., Gao, K. Q., Shawkey, M. D. and Gabbott, S. 2016. The plumage and colouration of an enantiornithine bird from the early cretaceous of china. *Palaeontology*, **60**, 55–71.

Pickrell, J. 2014. *Flying dinosaurs: How fearsome reptiles became birds*. Columbia University Press, 240 pp.

Pinheiro, F. L., Prado, G., Ito, S., Simon, J. D., Wakamatsu, K., Anelli, L. E., Andrade, J. A. F. and Glass, K. 2019. Chemical characterization of pterosaur melanin challenges color inferences in extinct animals. *Scientific Reports*, **9**, 15947.

Pralea, I. E., Moldovan, R. C., Petrache, A. M., Ilies, M., Heghes, S. C., Ielciu, I., Nicoara, R., Moldovan, M., Ene, M., Radu, M., Uifalean, A. and Iuga, C. A. 2019. From extraction to advanced analytical methods: the challenges of melanin analysis. *International Journal of Molecular Sciences*, **20**, 3943.

Rogers, C. S., Astrop, T. I., Webb, S. M., Ito, S., Wakamatsu, K. and McNamara, M. E. 2019. Synchrotron X-ray absorption spectroscopy of melanosomes in vertebrates and cephalopods: implications for the affinity of *Tullimonstrum*. *Proceedings of the Royal Society B*, **286**, 20191649.

Rogers, C. S., Webb, S. M. and McNamara, M. E. 2021. Synchrotron x-ray fluorescence analysis reveals diagenetic alteration of fossil melanosome trace metal chemistry. *Palaeontology*, **64**, 63–73.

Romano, M. and Pignatti, J. 2021. The fossil merchant from Verona: the first written testimony of paleontological forgery in Italy. *Rendiconti Online della Società Geologica Italiana*, **55**, 54–63.

Ronchi, A., Sacchi, E., Romano, M. and Nicosia, U. 2011. A huge caseid pelycosaur from north-western Sardinia and its bearing on European Permian stratigraphy and palaeobiogeography. *Acta Palaeontologica Polonica*, **56**, 723–738.

Rossi, V. and Castelli, S. 2023. Photogrammetry and UV photography of Trideninosaurus antiquus (MGP-PD 2657). MorphoSource. https://www.morphosource.org/projects/000587003

Rossi, V., McNamara, M. E., Webb, S. M., Ito, S. and Wakamatsu, K. 2019. Tissue-specific geometry and chemistry of modern and fossilized melanosomes reveal internal anatomy of extinct vertebrates. *Proceedings of the National Academy of Sciences*, **116**, 17880–17889.

Rossi, V., Webb, S. M. and McNamara, M. E. 2020. Hierarchical biota-level and taxonomic controls on the chemistry of fossil melanosomes revealed using synchrotron X-ray fluorescence. *Scientific Reports*, **10**, 8970.

Rossi, V., Unitt, R., McNamara, M. E., Zorzin, R. and Carnevale, G. 2022. Skin patterning and internal anatomy in a fossil moonfish from the Eocene Bolca Lagerstätte illuminate the ecology of ancient reef fish communities. *Palaeontology*, **65**, e12600.

Rowe, T., Ketcham, R. A., Denison, C., Colbert, M., Xu, X. and Currie, P. J. 2001. The *Archaeoraptor* forgery. *Nature*, **410**, 539–540.

Saha, A., Arora, R., Yakovlev, V. V. and Burke, J. M. 2011. Raman microspectroscopy of melanosomes: the effect of long term light irradiation. *Journal of Biophotonics*, **4**, 805–813.

Scheyer, T. M., Oliveira, G. R., Romano, P. S., Bastiaans, D., Falco, L., Ferreira, G. S. and Rabi, M. 2023. A forged 'chimera' including the second specimen of the protostegid sea turtle *Santanachelys gaffneyi* and shell parts of the pleurodire Araripemys from the Lower Cretaceous Santana Group of Brazil. *Swiss Journal of Palaeontology*, **142**, 1–11.

Selden, P. A., Olcott, A. N., Downen, M. R., Ren, D., Shih, C. and Cheng, X. 2019. The supposed giant spider *Mongolarachne chaoyangensis*, from the Cretaceous Yixian Formation of China, is a crayfish. *Palaeoentomology*, **2**, 515–522.

Slater, T. S., Ito, S., Wakamatsu, K., Zhang, F., Sjövall, P., Jarenmark, M., Lindgren, J. and McNamara, M. E. 2023. Taphonomic experiments reveal authentic molecular signals for fossil melanins and verify preservation of phaeomelanin in fossils. *Nature Communications*, **14**, 5651.

Sosiak, C. E., Borowiec, M. L. and Barden, P. 2023. Retraction: an Eocene army ant. *Biology Letters*, **18**, 20220398.

Spindler, F., Werneburg, R., Schneider, J. W., Luthardt, L., Annacker, V. and Rössle, R. 2018. First arboreal 'pelycosaurs' (Synapsida: Varanopidae) from the early Permian Chemnitz Fossil Lagerstätte, SE Germany, with a review of varanopid phylogeny. *PalZ*, **92**, 315–364.

Spindler, F., Werneburg, R. and Schneider, J. W. 2019. A new mesenosaurine from the lower Permian of Germany and the postcrania of *Mesenosaurus*: implications for early amniote comparative osteology. *PalZ*, **93**, 303–344.

Stone, R. 2010. Altering the past: China's faked fossils problem. *American Association for the Advancement of Science*, **330**, 1740–1741.

Tomasini, E. P., Halac, E. B., Reinoso, M., Di Liscia, E. J. and Maier, M. S. 2012. Micro-Raman spectroscopy of carbon-based black pigments. *Journal of Raman Spectroscopy*, **43**, 1671–1675.

Vahur, S., Teearu, A., Peets, P., Joosu, L. and Leito, I. 2016. ATR-FT-IR spectral collection of conservation materials in the extended region of 4000–80 cm^{-1}. *Analytical & Bioanalytical Chemistry*, **408**, 3373–3379.

Van Loon, A. and Boon, J. J. 2004. Characterization of the deterioration of bone black in the 17th century Oranjezaal paintings using electron-microscopic and micro-spectroscopic

imaging techniques. *Spectrochimica Acta Part B: Atomic Spectroscopy*, **59**, 1601–1609.

Vinther, J. 2015. A guide to the field of palaeo colour: melanin and other pigments can fossilise: reconstructing colour patterns from ancient organisms can give new insights to ecology and behaviour. *BioEssays*, **37**, 643–656.

Vinther, J., Briggs, D. E. G., Prum, R. O. and Saranathan, V. 2008. The colour of fossil feathers. *Biology Letters*, **4**, 522–525.

Wang, X. 2013. Mortgaging the future of Chinese paleontology. *Proceedings of the National Academy of Sciences*, **110**, 3201.

Yang, Z., Jiang, B., McNamara, M. E., Kearns, S. L., Pittman, M., Kaye, T. G., Orr, P. J., Xu, X. and Benton, M. J. 2019. Pterosaur integumentary structures with complex feather-like branching. *Nature Ecology & Evolution*, **3**, 24–30.

Zhang, F., Kearns, S. L., Orr, P. J., Benton, M. J., Zhou, Z., Johnson, D., Xu, X. and Wang, X. 2010. Fossilized melanosomes and the colour of Cretaceous dinosaurs and birds. *Nature*, **463**, 1075–1078.

Zhou, Z., Clarke, J. A. and Zhang, F. 2002. *Archaeoraptor*'s better half. *Nature*, **420**, 285.